

Article

Photocatalytic Degradation of Methylene Blue from Aqueous Solutions by Using Nano-ZnO/Kaolin-Clay-Based Nanocomposite

Shreya Modi ^{1,2}, Virendra Kumar Yadav ³ , Daoud Ali ⁴, Nisha Choudhary ^{3,*}, Saud Alarifi ⁴, Dipak Kumar Sahoo ⁵ , Ashish Patel ^{3,*}  and Madhusudan Hiraman Fulekar ⁶

¹ School of Nanosciences, Central University of Gujarat, Gandhinagar 382030, Gujarat, India; shreyamodi20@gmail.com

² Department of Microbiology, Shri Sarvajanik Science College, Hemchandracharya North Gujarat University, Patan 384001, Gujarat, India

³ Department of Life Sciences, Hemchandracharya North Gujarat University, Patan 384265, Gujarat, India; yadava94@gmail.com

⁴ Department of Zoology, College of Science, King Saud University, P.O. Box 2455, Riyadh 11451, Saudi Arabia

⁵ Department of Veterinary Clinical Sciences, College of Veterinary Medicine, Iowa State University, Ames, IA 50011, USA; dsahoo@iastate.edu

⁶ Center of Research for Development, Parul University, Vadodara 391760, Gujarat, India

* Correspondence: nishanaseer03@gmail.com (N.C.); uni.ashish@gmail.com (A.P.)

Abstract: Dyes are toxic organic compounds released as effluent from various industries that need proper treatment as they pose serious hazards to the environment and living beings, including humans. Nanocomposites can be employed as photocatalysts for the elimination of such organic compounds from wastewater. One such attempt is made in this present research study, where a zinc-based nanocomposite has been fabricated for the elimination of the methylene blue dye (MB). For the development of nanocomposite, zinc oxide nanoparticles (ZnONPs) were prepared to utilize *Allium sativa* peel (garlic skin) extract, which was further processed to develop ZnO/kaolin clay NC. ZnONPs and ZnO/kaolin clay NC formation have been confirmed by UV-Vis spectral bands at 379 nm and 423 nm. The NC was rod-shaped, with width of 60–100 nm and length of 200–800 nm and an average size of 50.0 ± 0.58 nm. Both materials were compared for their efficacy in photocatalytic degradation of the MB under solar light irradiation. ZnONPs removed 65% of MB, whereas the degradation efficiency of ZnO/clay NC was calculated to be 96% for 10 ppm MB. A kinetics study for photocatalytic degradation of MB using both nanomaterials showed that the photocatalytic degradation followed the pseudo-first-order (PFO) type of reaction. This investigation represents an expeditious, lucrative, ecological, and appropriate technique for the fabrication of functional nanomaterials for the remediation of diverse organic pollutants.

Keywords: nanocomposite; kaolin clay; photocatalytic degradation; *Allium sativa*; methylene blue



Citation: Modi, S.; Yadav, V.K.; Ali, D.; Choudhary, N.; Alarifi, S.; Sahoo, D.K.; Patel, A.; Fulekar, M.H. Photocatalytic Degradation of Methylene Blue from Aqueous Solutions by Using Nano-ZnO/Kaolin-Clay-Based Nanocomposite. *Water* **2023**, *15*, 3915. <https://doi.org/10.3390/w15223915>

Academic Editors: Nina Kaneva and George Tzvetkov

Received: 9 October 2023

Revised: 4 November 2023

Accepted: 7 November 2023

Published: 9 November 2023



Copyright: © 2023 by the authors. Licensee MDPI, Basel, Switzerland. This article is an open access article distributed under the terms and conditions of the Creative Commons Attribution (CC BY) license (<https://creativecommons.org/licenses/by/4.0/>).

1. Introduction

Every year, a huge amount of dyes are released into the environment from the textile, food, and other industries, which leads to harmful effects on living organisms, including aquatic organisms [1]. Dye-contaminated water consumption may cause diseases like skin irritation and, in prolonged cases, may lead to cancer [2]. The currently available approaches for dye removal, for instance, coagulation–flocculation, electroplating, precipitation, sedimentation, filtration (micro-, ultra-, and nanofiltration), etc., are not that effective as some are expensive, energy intensive, generate hazardous products and residue, and require longer periods for the remediation of dyes [3]. So, there is an immediate requirement for advanced techniques like nanotechnology for efficient and effective remediation of dyes [4,5].

The nanotechnology field is growing continuously with tremendous speed and has contributed applications in almost every field of science [6]. Nanoparticles are prime materials possessing a high surface area to volume ratio, small particle size ranging from 1–100 nm, and high surface energies and are thus utilized in a wide range of scientific areas, but when they are used in a pure form, they tend to agglomerate very quickly [7]. So, this problem could be overcome by developing a nanocomposite in which nanoparticles are supported within the interlamellar spaces of polymer/clay or by another metal matrix on their external surfaces [8,9]. In the domain of modern science and technology, various nanocomposite compounds having multifunctional properties are being developed and applied in the sectors of energy, electronics, biomedicine, biotechnology, and wastewater treatment [10–12].

Generally, composite materials provide reinforcements to the matrix, enhancing the thermal-electrical conductivity, ductility, hardness, tensile strength, and durability of the nanocomposite materials [13,14]. Nanocomposites are multiphase solid materials reinforced with NPs with either one, two, or three dimensions below 100 nm [15,16]. A nanocomposite consists of two phases, i.e., a continuous phase called the “matrix” and a discontinuous phase called “reinforcement” [17,18]. Further, these two phases may be inorganic–inorganic, organic–organic, or inorganic–organic [19–21]. The development of NC materials helps overcome the shortcomings of micron-scale reinforcements [22–24]. The physical, chemical, mechanical, and electrical properties of a material are drastically enhanced by the addition of a small amount of NPs in the matrix [25,26]. Furthermore, incorporating these nanoadditives in nanocomposites could enhance the properties such as heat distortion temperature, modulus, barrier properties, and flexural strength of the composite [27–30].

One of the most widely used non-toxic, eco-friendly matrices for developing nanocomposite is clay [31]. Unmodified natural clays and functionalized clays with an internal lamellar structure, large surface area and high porosity, and great adsorption potential have been utilized for the elimination of pollutants (organic and inorganic) from aqueous media [32]. Kaolin is a dioctahedral 1:1 layered clay chiefly composed of mineral kaolinite ($\text{Al}_1\text{Si}_2\text{O}_5(\text{OH})_4$) [33], which is extensively used as a filler in rubber, plastics, paper, and paint industries [34]. The layered kaolin clay contains two sheets: one is a tetrahedral sheet where atoms of silicon [35,36] are tetrahedrally coordinated with oxygen atoms, and the second is an octahedral sheet in which atoms of aluminum metal are octahedrally coordinated with hydroxy groups and common apical oxygens from the tetrahedral silica sheet [37]. Adsorption by clays has become an attractive and promising wastewater treatment technology because of their abundant availability and cost effectiveness. The easy availability of clay and its non-toxic and recyclable nature are some of the basic advantages of clay [38–41].

Consequently, the efficiency of nanocomposites formed from NC developed from a photocatalytic material such as TiO_2 or ZnO will be enhanced since the material will have features of NPs and catalytic properties. Nanocomposite material developed from clay and ZnONPs is one of the most promising materials for the photocatalytic disintegration of dyes [42]. Several investigators have developed nanocomposites from clay like montmorillonite (MMT) [43] and halloysite (HC) [44–46]. Furthermore, a few researchers have employed NPs of silver and zinc oxide for surface modification of clay and the subsequent development of nanocomposites.

A group of investigators led by Boushehrian developed kaolin/ CuFe_2O_4 NC and applied it for the remediation of cationic dyes [47]. A team led by Choudhary developed a montmorillonite/Ag nanocomposite and utilized it for the remediation of methylene blue dye from wastewater [48]. Gnanamoorthy and their group developed CuNiO_2 and rGO nanocomposites, which have been applied for the elimination or photocatalytic degradation (PD) of methylene blue from aqueous solutions [49]. Bayomie et al., 2020 have also removed methylene blue dye (MB) from an aqueous solution using fava bean peel waste [50]. Massaro and their team reported the one-pot synthesis of ZnONPs supported

on halloysite nanoclay (HNT@ZnO hybrid). The investigators further reported that the presence of clay enhanced the UV–Vis spectral potential of the ZnONPs [51]. Mustapha and their team developed a kaolin and ZnONP composite where ZnONPs were prepared by the sol–gel technique, and ZnONPs were further decorated on the surface of kaolin by applying the wet impregnation method. The surface area of the developed nanocomposite was $31.8 \text{ m}^2/\text{g}$, as confirmed by Brunauer–Emmett–Teller (BET) [52]. A team led by Mamulová developed a nanocomposite of ZnONPs and kaolin clay by varying the ZnONPs by weight, i.e., 10 wt.%, 30 wt.%, and 50 wt.%, by applying the hydrothermal technique. Furthermore, the investigators calcinated the nanocomposite at 600°C to lead to the kaolinite–metakaolinite phase transformation [53]. Recently, Choudhary and their team developed a nanocomposite made up of ZnONPs loaded on halloysite nanoclay, which was used for the elimination of MB efficiently [46]. In addition to this, the photodegradation of MB was also investigated by Modi and their team, for instance, in one of the attempts, a bacterial consortium along with ZnONPs [54] was used, while in another attempt, ZnONPs and doped ZnONPs (tungsten and antimony) were used [55].

The present investigation emphasizes the development of biocompatible zinc oxide nanoparticles using garlic peel extract. Another objective was to develop a simple technique for the preparation of ZnONP/kaolin nanocomposite. The developed nanocomposite was characterized by analytical instruments for detailed information. Another objective was to evaluate the efficacy of the fabricated nanocomposite for the photocatalytic degradation of methylene blue dye from aqueous solutions. The final objective was to assess the effect of pH, initial concentration, and contact time on the photocatalytic degradation of methylene blue dyes. Such a method of waste-mediated synthesis and remediation of dyes by using non-toxic material makes the process environmentally friendly.

2. Experimental

2.1. Materials

Kaolin clay (SRL, Ahmedabad, Gujarat, India), acetic acid (Merck, Mumbai, India), methylene blue (Molychem, Ahmedabad, Gujarat, India), zinc chloride (Merck, Mumbai, India), sodium hydroxide pellets (Merck, Mumbai, India), Whatman filter paper no 42 (Axiva, Mumbai, India), ethanol (95% Shenzhen, China), and double distilled water (ddw) were used.

2.2. Methods

2.2.1. Synthesis of Zinc Oxide Nanoparticles

About 50 g of garlic peel (*Allium sativa*) was collected from a vegetable market (Gandhinagar, Gujarat, India). The garlic peel was dried properly in an oven at 40°C . Further, about 10 g of dried garlic peel powder was soaked in 80% 100 mL of ethanol. The mixture was continuously stirred for 24 h on a magnetic stirrer and heated at 60°C . Further, the extract was passed through a Whatman filter paper no 42 to obtain the filtrate while the residue was discarded. The garlic extract was stored in a reagent bottle for future use.

Furthermore, about 200 mL of 2 mM ZnCl_2 aqueous solution was taken in a beaker, to which 30 mL of garlic extract was added dropwise. The mixture was continuously stirred on a magnetic stirrer during the reaction. Further, the mixture changed its color within 30 min, and the reaction was stirred for 4 h. The pH was adjusted from 8.5 to 9 at this stage using sodium hydroxide and the stirring speed at 300 rpm. Further, the mixture was centrifuged at 6000 rpm for 7 min to obtain the residue. The obtained white precipitate was washed 2–3 times with ddw and once with ethanol in order to eliminate impurities. Finally, the white precipitate was dried in an oven at 80°C overnight, then calcinated at 600°C for 4 h by increasing the temperature by $5^\circ\text{C}/\text{min}$. The detailed process was discussed earlier by Modi and Fulekar [56].

2.2.2. Development of Clay Nanocomposite

Kaolin clay was sieved using a 50-micron mesh and then mixed with 50 mL of 1% acetic acid. About 2 g of sieved kaolin was weighed, mixed with 50 mL of 1% acetic acid solution, and stirred for 30 min. At the same time, 2 g of ZnONPs was also weighed and dispersed in 50 mL of 1% acetic acid solution under stirring conditions for 30 min. Both the solutions were then mixed, and stirring was continued for another 30 min. Afterward, the mixed solution was subjected to sonication for 60 min at 60 °C. Sonication was followed by a continuous stirring of 8 h at 400 rpm. In later stages, the solution was centrifuged at 6000 rpm for 15 min, and the obtained solid pellet was washed with Milli-Q water five times. The washing step was followed by drying the pellet at 60 °C overnight. In this manner, ZnO NC was obtained.

2.3. Preparation of Methylene Blue Dye Aqueous Solution and Dye Removal

The photodegradation of MB was determined in a simple reactor under exposure to solar light. About 30 mg of synthesized and developed ZnONP/kaolin clay NC was added to a 250 mL glass vessel having around 100 mL of MB solution with different concentrations (10 ppm, 25 ppm, 50 ppm). This solution was kept in sunlight under stirring conditions (~400 rpm). Every 15 min, 5 mL of the sample was pipetted out for up to 120 min. The acquired samples were then analyzed to determine the absorption spectrum at 665 nm and wavelength scan (200–700 nm). A dye removal study was also carried out based on the pH and dosage of the nanocomposites. The sample was also examined by a gas chromatography–mass spectroscopy investigation (GC-MS) to find the degradation pathway at each step.

3. Characterization of Nanoparticles and Nanocomposites

The synthesized nanocomposites were characterized by an electron microscope (field emission scanning and transmission), UV-Vis spectroscopy, Fourier-transform infrared (FTIR), and X-ray diffraction (XRD). About 1 mg nanocomposite was taken in 10 mL of ddw, and sonication was performed by a Sonar-made (40 kHz) ultrasonicator (Sonar, 40 kHz, Vadodara, India). Further, the finely dispersed developed nanocomposite was used for the UV-Vis analysis and TEM. The UV-Vis analysis was performed by a UV-Vis spectrophotometer (Halo DB-20, Double-beam, Dynamics) in the 200–800 nm range. Finely dispersed nanocomposite in ddw was poured over carbon-coated Cu grids by the drop-casting technique for visualization of micrographs by TEM. The detailed morphological features were revealed using FEI, Technai G2-Twin (New York, NY, USA). By using a solid KBr pellet technique, the FTIR investigation was carried out using a Perkin Elmer Model SP-65 (Markham, ON, Canada) instrument in the IR regions of 400–4000 cm^{-1} at a resolution of 1 nm. For the surface morphological features, FESEM analysis was carried out where a pinch of sample was placed on carbon tape, which in turn was kept on an aluminum stub. The sample was kept in the sample holder, and imaging was carried out using a NOVO Nanosem, 450 (FEI, USA) at different resolutions. The elemental constituents of the samples were identified by using an electron diffraction spectroscope (Oxford make) fitted with the FESEM. The phase identification of the samples was carried out by XRD. The powder samples were analyzed by using a D8 Advance (Bruker, Mannheim, Germany) in the 2θ of 10–80°, step size = 0.02, time = 5 s/step, voltage = 40 kV, and current = 30 mA.

4. Results and Discussion

4.1. Chemical Composition of Garlic Peel Extracts

From the various pieces of literature, it has been found that garlic peel extract has various bioactive compounds, for instance, total phenolic compounds (3910.98 ± 140.64 to $14,657.42 \pm 557.48$ mg gallic acid equivalent/100 g), total flavonoids (0.3768 ± 0.0269 to 0.9063 ± 0.0204 (mg/100 mL), total tannins (434.33 ± 7.52 to 1688.94 ± 4.68 mg tannic acid equivalent/g), and total anthocyanins (0.2885 ± 0.0386 to 1.3204 ± 0.0655 (mg/100 mL). The extracts from the garlic peel have shown compounds like garlic organosulfur compounds,

which are mainly divided into two parts, i.e., non-volatile precursors and volatile precursors. Further, the non-volatile precursors were mainly gamma-glutamyl-S-allyl-L-cysteine and S-allyl-L-cysteine sulfoxide (alliin). Meanwhile, thiosulfinate (allicin), volatile organosulfur compounds (methyl allyl disulfide, methyl allyl trisulfide), and water-soluble organosulfur compounds are the main volatile precursors [57–59].

4.2. Mechanism of Formation of ZnONP/Kaolin Composite

Mustafa and their team proposed a schematic method (Figure 1) for the development of the ZnONP/kaolin composite by using a sol–gel method followed by a wet impregnation method. First, the zinc acetate and NaOH formed a gel, which was later impregnated on the surface of kaolin [52].

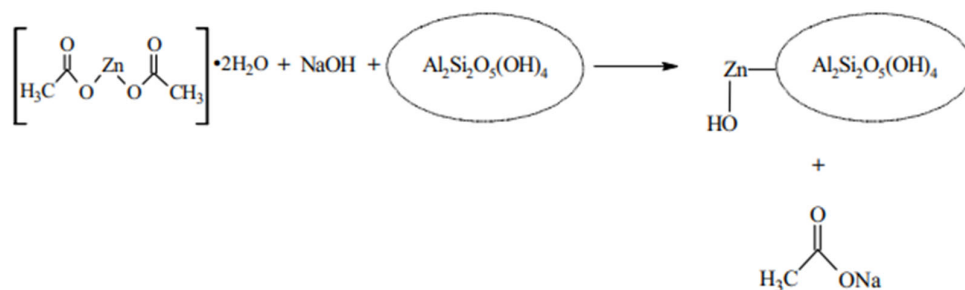


Figure 1. A schematic representation of the preparation of kaolin/ZnO nanocomposites adapted from [52].

The synthesized and developed ZnONPs and ZnO/clay NC were characterized using standard methods. The obtained results are represented below.

4.3. UV–Visible Spectroscopy

A typical UV–Vis spectrum of the developed nanocomposite dispersed in ddw prior to analysis is shown in Figure 2. The absorption bands of photocatalysts were 379 nm and 423 nm, respectively, for ZnONPs and ZnO/clay NC. From the analysis, it is assumed that the absorption edge and intensity shifted with the incorporation of composite material within ZnONPs due to quantum confinement effects [60]. Since UV is a surface plasmon resonance phenomenon, the surface and interface of the developed NC contribute an important role in light absorption. On the surface of nanomaterials, there are electron (e^-) clouds, capable of oscillating and absorbing electromagnetic radiation at a particular energy [61]. Khan and Fulekar also obtained a similar result for chemically synthesized ZnONPs [62].

4.4. FTIR Analysis of ZnONPs and ZnO/Clay NC

The infrared spectra for ZnONPs exhibited bands corresponding to the chemical bonds present in the ZnONPs. In Figure 3, both ZnONPs and the developed NC exhibit clear bands around $3700\text{--}3400\text{ cm}^{-1}$, assigned to the $\nu(\text{-OH})$ stretching. The $\nu(\text{-OH})$ stretching band in ZnONPs is broad, which starts at 3200 and ends at 3600 cm^{-1} , while this band became sharper in the NC, centered at 3673 cm^{-1} .

A broad band in the NC at 1100 cm^{-1} is assigned to the Si-O-Si/Si-O-Al present in the clay samples [63,64]. The band at 748 and 570 in the ZnONPs is due to the Zn-O. The band at 540 and 827 cm^{-1} in the NC is due to the Zn-O bond. This band is also due to the Al-O and Si-O bond in the NC, indicating the presence of aluminates and silicates coming from clay [65,66]. The bands at 1627 and 1875 cm^{-1} in ZnONPs and the NC are assigned to the OH group available in the materials.

The previous results obtained by Mamulová and their team were close to the current investigation for the developed clay NC. For the synthesized ZnONPs, bands were obtained at $\sim 420\text{ cm}^{-1}$ (Zn-O stretching). The bands of raw kaolin were obtained near 3600 cm^{-1} , corresponding to the inner octahedral structure of Al OH bonds. The bands at 1135, 787,

643, and 456 cm^{-1} were attributed to Si-O, while the bands at 999, 749, 679, and 522 cm^{-1} were attributed to Si O Al and the bands at 936 and 911 cm^{-1} were attributed to Al OH. The band at 1024 cm^{-1} corresponds to Si-O-Si. The band of Zn-O at 420 cm^{-1} was not observed in the clay NC as it was overlapped by the kaolin [53].

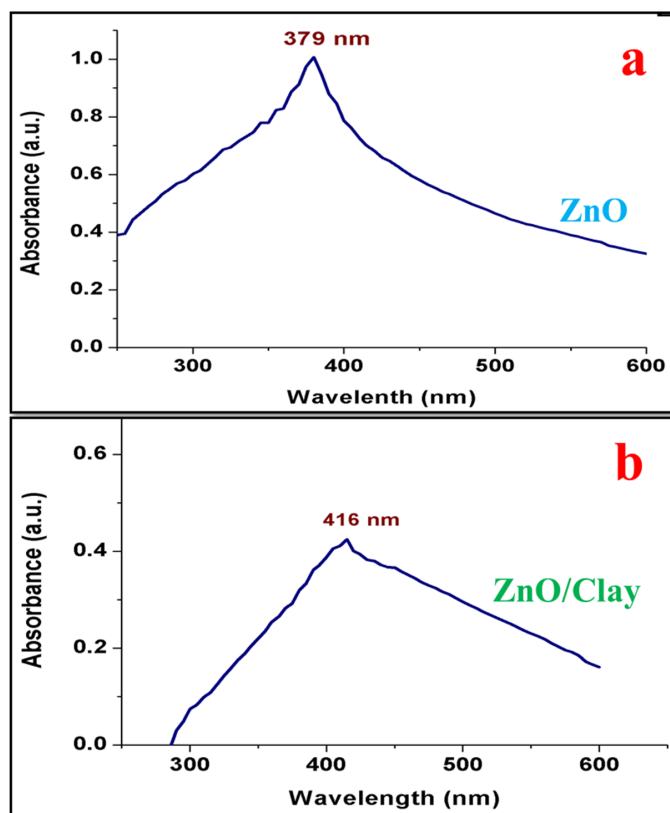


Figure 2. UV–Vis measurement of ZnONPs (a) and ZnO/clay NC (b).

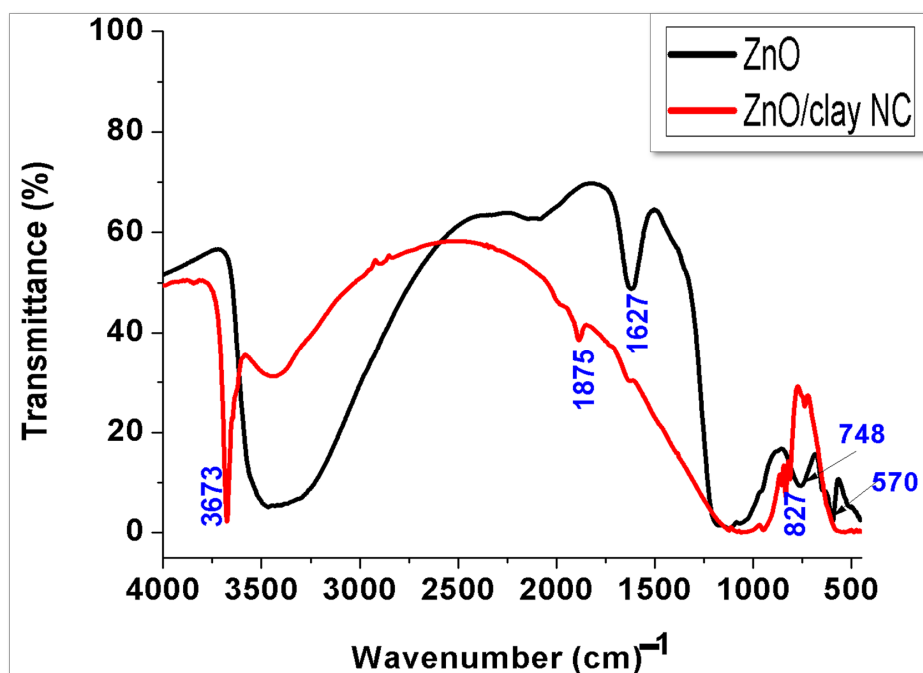


Figure 3. FTIR analysis of ZnONPs and ZnO/clay NC.

Mustapha and their team also obtained bands for the ZnONP/kaolin composite developed at different pHs, followed by calcination at 450 °C for 3 h. The characteristic bands for the developed composite were obtained at 3626–3696 cm⁻¹ and attributed to the OH vibration, that at 1034 cm⁻¹ was attributed to the Si–O–Si stretching vibration, those at 1114 cm⁻¹, 797, 787, 757, and 607 cm⁻¹ were attributed to the Si–O bonds, that at 914 cm⁻¹ was attributed to Ti–O–Si, and those at 775 and 522 cm⁻¹ were attributed to Si–O–Al. The band at 513 cm⁻¹ confirms the presence of Zn–O in the developed nanocomposite sample [52].

4.5. Phase Identification of ZnONPs, Kaolin, and Clay NC by XRD

Figure 4 is the XRD pattern of ZnONPs, kaolin clay, and ZnO and clay NC. The characteristic diffraction lines of ZnONPs are seen at 33, 35, 37, 46, and 56°. The phase of the ZnONPs was reported to be in good agreement with previous studies, for instance, Mustapha et al. [67], Modi et al. [55,68], and Mamulová et al. [53].

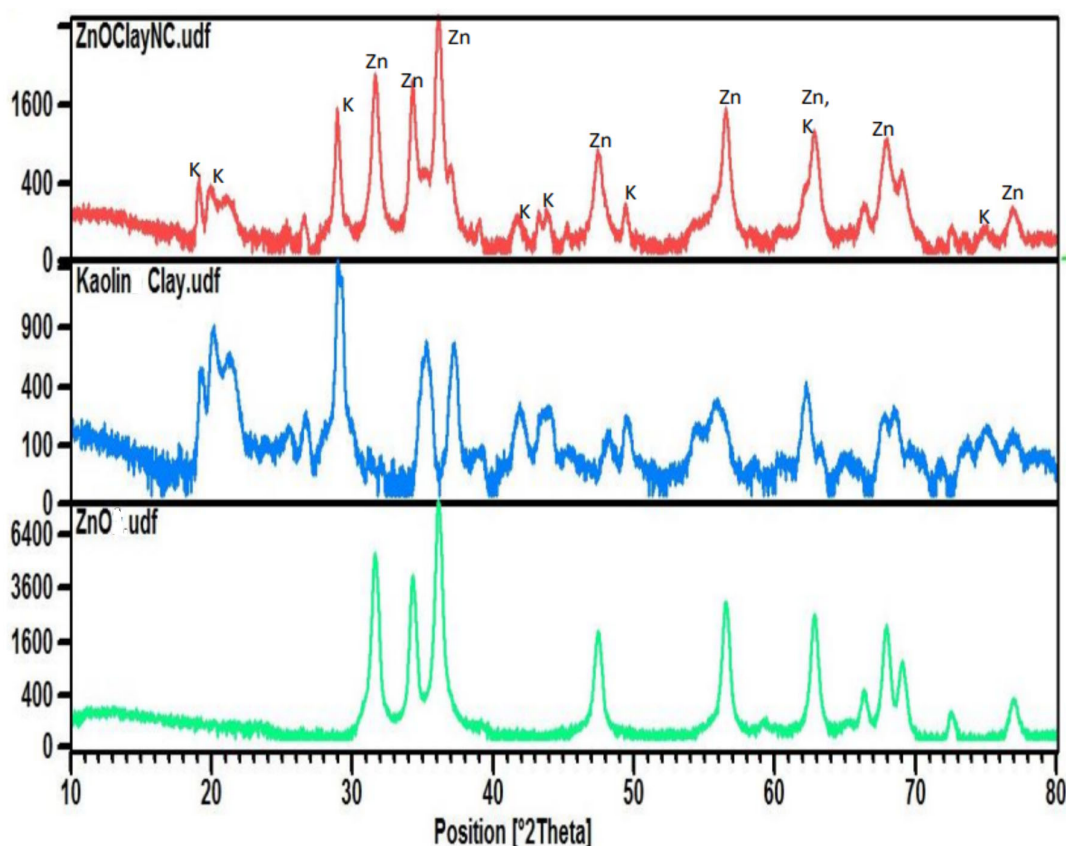


Figure 4. XRD pattern of ZnONPs, kaolin, and clay NC.

A broad diffraction line is shown from 20–25°, and a sharp diffraction line from 26–28°, attributed to the quartz and mullite phase in the clay. The diffraction line at 34° and 37° indicates the iron oxide phase, i.e., hematite [69] and magnetite [70].

The NC shows XRD diffraction lines from 20–22°, 27–29°, and at 41 and 42, while 33–38° is due to ZnONPs. Besides this, ZnO diffraction lines are also at 48° and 57° in the NC. A low-intensity diffraction line at 17° and a high-intensity peak at 29° suggest the presence of kaolinite in the developed clay NC, which was also suggested by Mustapha and their team, who obtained a low-intensity diffraction line at 12° and high-intensity diffraction lines at 26.8° [52].

Previously, Mamulová and their team also obtained ZnONP diffraction lines at 37.3° (100), 40.5° (002), and 42.5° (101), which are in close agreement with the current result. The major XRD diffraction lines for kaolinite in the kaolin were obtained at 13° and 29° while

we obtained diffraction lines at 17° and 29° along with a few small diffraction lines at 35° , 37° , and 65° . The diffraction lines for both ZnONPs and kaolinite, along with quartz, were present in the developed clay NC [53].

Mustapha and their team obtained low-intensity diffraction lines for the ZnONPs at 31.79° , 34.42° , 36.25° , and 56.60° corresponding to (100), (002), (101), (102), and (110) crystal planes. This further confirmed the presence of ZnONPs in the kaolin samples [52].

4.6. Morphological Analysis of NC by TEM

TEM images of the developed NC are exhibited in Figure 5a–d. The images reveal that the particles are rod-shaped with a width of 60–100 nm and a length of 200–800 nm. The layered structure of the clay could be clearly observed by TEM. Figure 5d clearly shows a single particle of NC, which is layered. Figure 5e exhibits the SAED pattern of the developed NC, indicating the less crystalline nature of NC. The SAED pattern does not show diffraction peaks, and the pattern of the concentric ring indicates that the ZnONPs are heterogeneously dispersed on the surface of kaolin. Figure 5f exhibits the particle size distribution (PSD) of NC, which indicates an average size of 50.0 ± 0.58 nm.

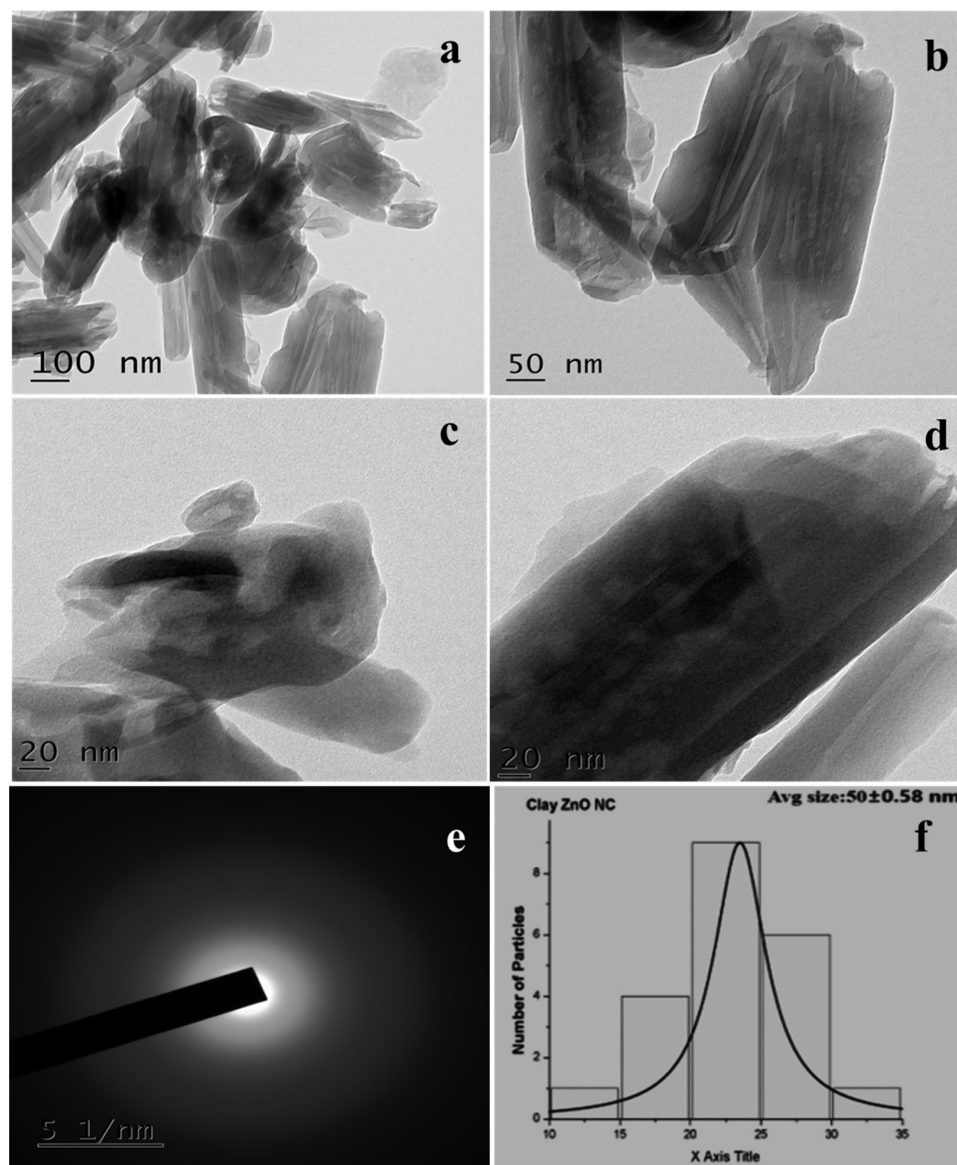


Figure 5. TEM images at different scales (a–d), SAED pattern (e), and histogram showing the particle size distribution (f) of clay NC.

Earlier, a team led by Mamulová reported the presence of ZnONPs on the surface of kaolin, where the morphology and density of ZnONPs varied with the temperature of calcination used. The further investigator concluded that ZnONPs are developed by the aggregates of crystallites having the form of larger or smaller slices. The TEM investigation showed the presence of spherical ZnONPs on the long rod-shaped kaolin [53]. A team led by Mustapha reported stacked hexagonal and plate-like structures that were less agglomerated [52]. Similar results were also obtained by Choudhary and Fulekar, where the investigators used ZnONPs on halloysite clay to develop NC [46].

4.7. Morphological Analysis of NC by FESEM

FESEM images of NC are shown in Figure 6a,b. Figure 6a shows NC at 200 nm, where the particles are layered floral shapes of size 100–800 nm. Figure 6b shows the image at 100 nm, where NC particles appear as layered structures with floral shapes. A similar structure was also reported by several investigators for kaolin particles. For instance, a team led by Mamulová reported that only a small number of ZnONPs are present in the different types of kaolin and ZnO nanocomposites where the matrix of kaolinite was quite empty [53]. The shape of the developed clay NC appeared to be crystals of gypsum/desert rose. Further, with the increasing concentration of ZnONPs (10–30%), there was an increase in the size of the ZnONPs. Moreover, in all the types of calcinated composite, the kaolinite was covered by a continuous layer of ZnONPs [53].

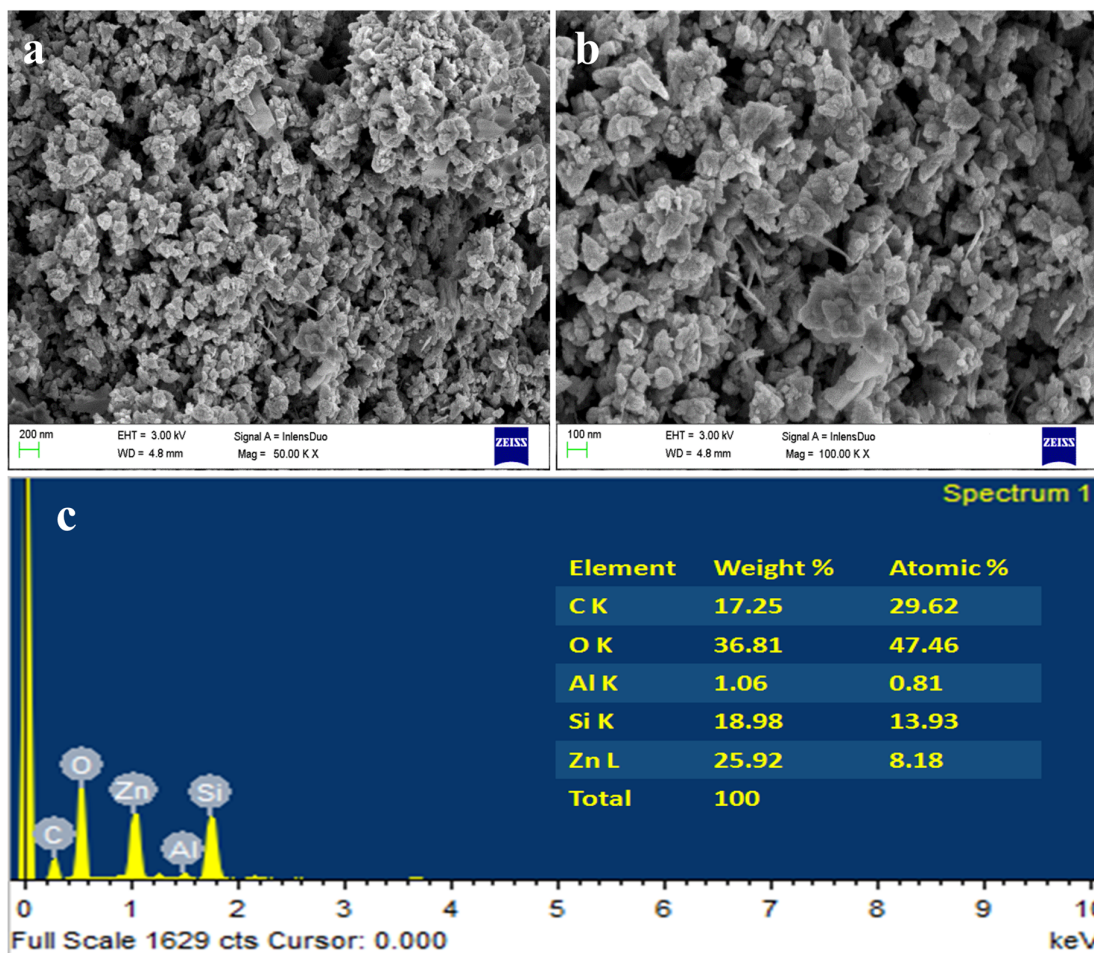


Figure 6. FESEM images at different magnifications (a,b) and EDS spectra and elemental table (c) of NC.

The EDS spectra and the elemental table are shown in Figure 6c, which shows peaks for carbon, O, Al, silicon, and Zn. A normal kaolin particle will have O, C, Al, and Si

along with H, but here, H could not be detected by the EDS analyzer. So, the presence of Zn suggests the doping of ZnONPs on the surface of the clay to form NC. Among all the elements, O is the most common, i.e., 36.81%, followed by Zn, i.e., 25.92%, and Si and C, i.e., 18.98% and 17.25%, respectively. It also has Al, which was about 1.06%. Besides this, no other elements were present in the samples, confirming the sample's purity.

The EDS spectra of Mamulová and their team showed the presence of C, O, Zn, and Si [53], while Mustapha and their team obtained peaks for O (26.3%), Na (4.92%), Zn (50.65%), Al (6.67%), Si (10.22%), and Fe (1.23%) [52].

4.8. Photocatalytic Degradation of Dye

4.8.1. Optimization of Variables in Photocatalytic Degradation

During the study, the effects of various parameters, for instance, the dosage of the photocatalyst [71], dye concentration (initial), and pH's effect on the PD of MB were studied using a ZnO nanocatalyst.

4.8.2. Effect of Catalyst Dose

In the PD analysis of dyes, the dosage of the nanophotocatalyst contributes a significant role due to the availability and cost of photocatalysts used for the efficient photodegradation of MB dye [72]. If a lesser amount of nanophotocatalyst is used, then there will be a reduction in the photocatalytic degradation of the respective dyes [73]. So, prior to performing dye degradation, optimization of their dosage is very economical when this is applied for degradation at a larger scale with minimal resources. Different dosages of ZnO/clay NC catalysts at varying concentrations from 100 to 600 ppm were collected into beakers containing 100 mL MB dye solution with a concentration of 10 ppm and pH 7.4. This sample was kept under solar light irradiation for a duration of 120 min, with a UV lamp, and the sample was stirred by a magnetic stirrer (400 rpm) while conducting the investigation. A graph of the percentage (%) degradation of MB dye for various catalyst dosages vs. time was plotted. It was observed that with the increase in photocatalyst dosage, the % degradation of MB dye increased, and the optimum value of catalyst dosage (300 ppm) at which the % degradation of MB dye was maximum (95.84%) for the duration of 120 min was reached. After that, a decrease in the optimum catalyst dose and % degradation was noticed, which could be explained by the presence of a large number of active sites on the catalyst surface and the penetration of light into the sample suspension. With the increase in the catalyst dosage, the number of active sites and surface area of nanocatalyst particles also increases. Consequently, there is an increase in the turbidity of the MB dye solution, which will decrease the light penetration into the solution due to the increased effect of scattering.

4.8.3. Effect of Initial Concentration of Dye

To analyze the effect of the initial concentration (IC) of dye on the PD process, various concentrations of MB dye were used during the study. The experiment was conducted with a fixed photocatalyst dose of 30 mg/100 mL at different ICs of MB dye of 10, 25, and 50 ppm (mg/L) prepared from a stock solution of 100 ppm. Data obtained during the experiment were plotted as the % degradation versus time in Figure 7. From the graph, it is obvious that the concentration of MB continuously decreased with the duration of contact time in all three concentrations of MB dye solution. In the case of the 10-ppm solution, the MB dye was degraded by almost 96% in 120 min, while when the concentration of MB in the solution was 25 and 50 ppm, the % degradation of dye was about 58% and 23%, respectively. Yadav et al., 2022 also removed MB from liquid media by using surface-modified ferrospheres recovered from coal fly ash [74]. Gnanamoorthy et al. also performed photocatalytic degradation of MB by using CuNiO₂ and their rGO nanocomposite and obtained efficient results [49]. Choudhary et al., 2021 developed a nanocomposite material from montmorillonite and silver NPs and applied them for the elimination of MB from liquid solutions. The investigators also used four variable concentrations of MB (25, 50,

100, and 200 ppm) and obtained a removal percentage of about 81–99%. The investigators have also obtained the highest removal percentage of MB with low ppm, i.e., 25, which was about 99.9%, and the lowest was with the highest ppm, i.e., 200 ppm, about 81.4% [48]. Tsade et al., 2021 efficiently removed MB from wastewater by using periodate-modified nanocellulose [75]. Massaro and their team photocatalytically removed methyl orange and rhodamine B from aqueous solution by using ZnONPs (avg size 3.9 ± 0.8 nm) decorated on halloysite nanotubes. The MO dye was completely photocatalytically degraded within 3 min with all the doses of photocatalyst, while the RhB dye was photocatalytically degraded after 30 min [51]. Mamulová and their team utilized the composite developed from kaolin and ZnONPs where the conc. of ZnO varied from 10–30%, and the calcination temperature of kaolin varied from 100–1200 °C. Further, the investigators used these clay NCs to eliminate acridine orange 7 from wastewater under photocatalytic conditions. About 60% of acridine orange 7 (AO7) was photodegraded from the solution within 30 min and 95% after 60 min by using the developed clay NC [53]. Mustapha and their group utilized a kaolin/ZnONP composite for the remediation of biological oxygen demand, chemical oxygen demand, and removal of Cr and Fe ions at different pH, dosages, etc. [52].

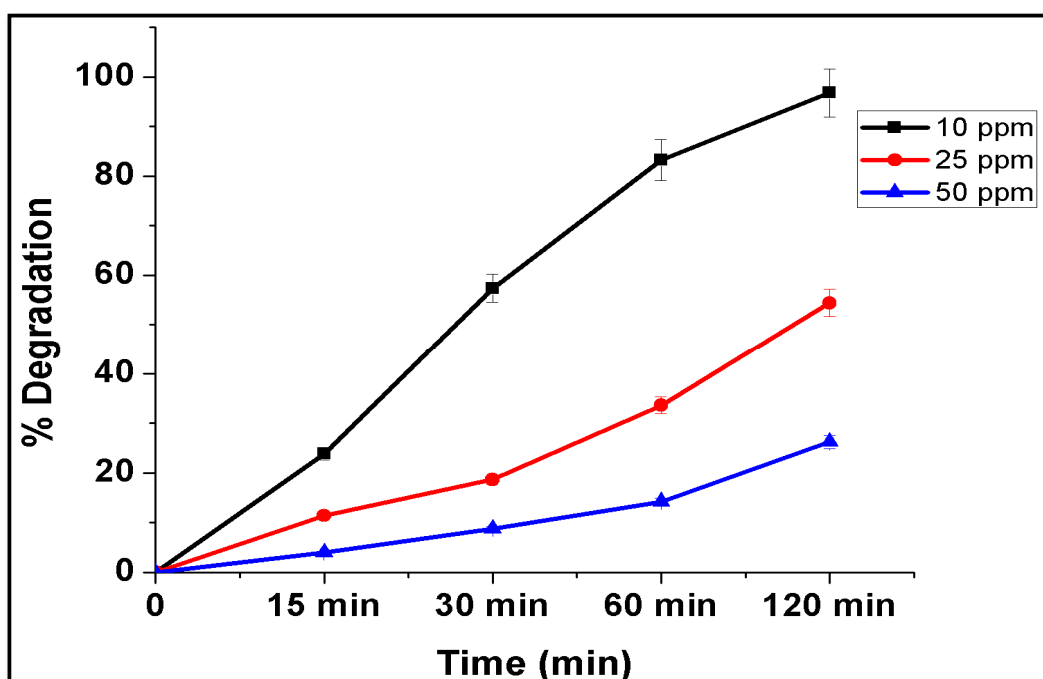


Figure 7. Graphical representations of the effect of initial concentration on dye.

From the results, the percentage degradation of MB dye decreases as the IC of the dye increases. It can be stated that as the concentration of dye increases, more reactants and reaction intermediates are adsorbed on the surface of photocatalysts, and this develops a layer on the surface; hence, it will minimize the production of hydroxyl radicals (OH). Apart from this, a high concentration of dye also increases the turbidity of the solution, which will block the photons from activating the photocatalyst. Furthermore, as the strength of the MB increases, the photons are intercepted before they can reach the surface of the nanocatalyst, and the length of the path of a photon entering into the MB solution is decreased [76]. Gnanamoorthy et al., 2022 have also proposed a similar hypothesis for MB remediation in aqueous solutions using nanocomposite material [49].

4.8.4. Effect of pH

To control the photodegradation process, pH is one of the crucial factors. During the study, the effect of pH on the PD efficiency of the dye samples was investigated at pH

3, 5, 7, 9, and 11 with 100 mL of 10 ppm IC of MB and a dose of 30 mg/L of ZnO/clay photocatalyst. The pH of the MB solution was adjusted by using 0.1 M HCl and 0.1 M NaOH before the investigations and results are shown in Figure 8. From the graph, it is clear that the dye was removed continuously at all pH levels for 120 min. The degradation percentage of MB at various pH levels was almost the same, i.e., 86–96%, but at 5 pH, degradation was marginally higher. The lowest degradation of MB was observed at 3 pH, i.e., 82, which could be due to the formation of H⁺ ions in acidic conditions, which may lead to the desorption of MB from the catalyst surface. Badeenezhad et al., 2019 also reported MB dye removal from wastewater by using natural clinoptilolite and clinoptilolite functionalized by IONPs [77]. Bayomie et al., 2020 also reported efficient results of MB elimination from aqueous solutions using banana peel waste [50]. Table 1 shows the PD of MB by several investigators using nanocomposite under UV light.

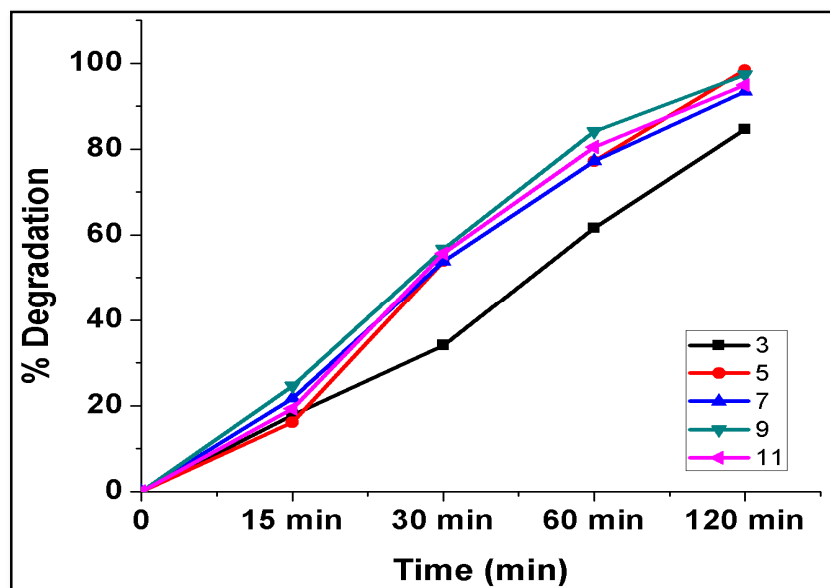


Figure 8. Graphical representation of the effect of pH on dye degradation of MB.

Table 1. PD of MB by several investigators using nanocomposite and biosorbent under UV and visible light.

Nanocomposite/Nanomaterials	Size (nm)	Removal Percentage	Concentration of Dye (ppm)	Time (Minutes)	References
MMT/Ag	1–2 microns	99.9%	25	30	[48]
Halloysite/ZnONPs	40–200 (diameter)	97.5	25	15	[46]
ZnONPs	7	82.01	10	-	
W-doped ZnONPs	18	88.21	10	-	[55]
Sb-doped ZnONPs	9.55	90.06	10	120	
ZnONPs	40–100	100	300	60	[78]
NaOH-activated incense sticks, ash		69.74	200	60	[79]
Fe ₃ O ₄ @SiO ₂ /TiO ₂ @WO ₃		92.77		60	[9]
Na periodate-modified nanocellulose (NaIO ₄ NC) from <i>Eichhornia crassipes</i>	Several microns	90.91 mg·g ⁻¹ 78.1%	30	60	[80]

Table 1. Cont.

Nanocomposite/Nanomaterials	Size (nm)	Removal Percentage	Concentration of Dye (ppm)	Time (Minutes)	References
Self-assembled cylindrical graphene–CNTs	Width: 20–40 nm Length: several microns	81.97 mg/g 97%	10		[81]
CdSe-TiO ₂ NPs	TiO ₂ : 20 ± 1 nm CdSe: 3.0 ± 0.2 nm	67%	10	60	[82]
Chitosan/Fe ₃ O ₄ /graphene oxide (CS/Fe ₃ O ₄ /GO) NC	IONPs: 30–40 nm	30.10 mg/g (by Langmuir) 90–100%		10–40	[83]
Boron nitride nanosheets @ polyvinylidene fluoride		142.86 mg/g 100%	10		[84]
NZVI-impregnated nanoclay	72.4 nm	~100	40	120	[85]
Clinoptilolite modified by iron oxide NPs	Microns	98%	200	45 (optimum)	[77]
CuO/ZnO nanophotocatalysts	10–55 nm	97%		85	[86]
Hydrotalcite-supported NZVI	90 nm to several microns	81 mg/g 99.6%	40	30	[87]
ZnONP loaded on bacterial consortium		95.46%	10	4320	[54]
Zeolite imidazolate frameworks (ZIF-67) @ co-layered double hydroxide	1 μm diameter, thickness ~40 nm	57.24 mg/g 79.9%	25	100	[88]
Mn-doped ZnO nanocomposites	50 nm	70%	0.1 mM	60	[89]
Yb ³⁺ -Zn ²⁺ substituted M-type hexaferrites	16–17 nm	96.1 %		90	[90]
ZnONPs@cellulose nanocrystals NC	59.51	88.62%	10	120	[68]
X-CuTiAP (en, trien, ETA, and DMA) nanospheres	Below 100	33–73	1 mM in 100 mL	50–60	[91]

4.8.5. Photocatalytic Activity and Mechanism

Solar radiation has the crucial advantage of being an inexhaustible free energy source without any toxic effects on our environment. ZnO photocatalysts absorb a small percentage of the total sunlight for their photocatalytic activation [92]. The photocatalytic activity of ZnO nanomaterials come about due to the generation of electron–hole pairs by absorbing an amount of energy that is either greater than or equal to the energy gap. The e[−] being generated is transported to the conduction band (CB), and the hole remains in the valence band (VB). Thus generated, an electron–hole pair may relink some energy to reach a metastable state (MtS). Mir et al., 2017 also degraded MB photocatalytically but with CdSe-TiO₂ NPs [82]. The electron, resent in an MtS, interacts with O₂ vacancies to produce superoxide ions, while the hole in an MtS interacts with water or hydroxide ions to produce highly reactive hydroxyl radicals at the catalyst–water interface [82]. Figure 9 shows a possible MB dye degradation mechanism by clay NC.

4.8.6. Chromophoric Group Degradation: First Degradation Pathway

Sulphydryl is converted to sulfoxide, and the central aromatic heterocycle opens during electronic reorganization. The intermediate products of MB degradation included 2-amino-5-(N-methyl formamide) benzene sulfonic acid (*m/z* = 230), 2-amino-5-(methyl

amino)-hydroxybenzene sulfonic acid ($m/z = 218$), benzene sulfonic acid ($m/z = 158$), and phenol ($m/z = 94$).

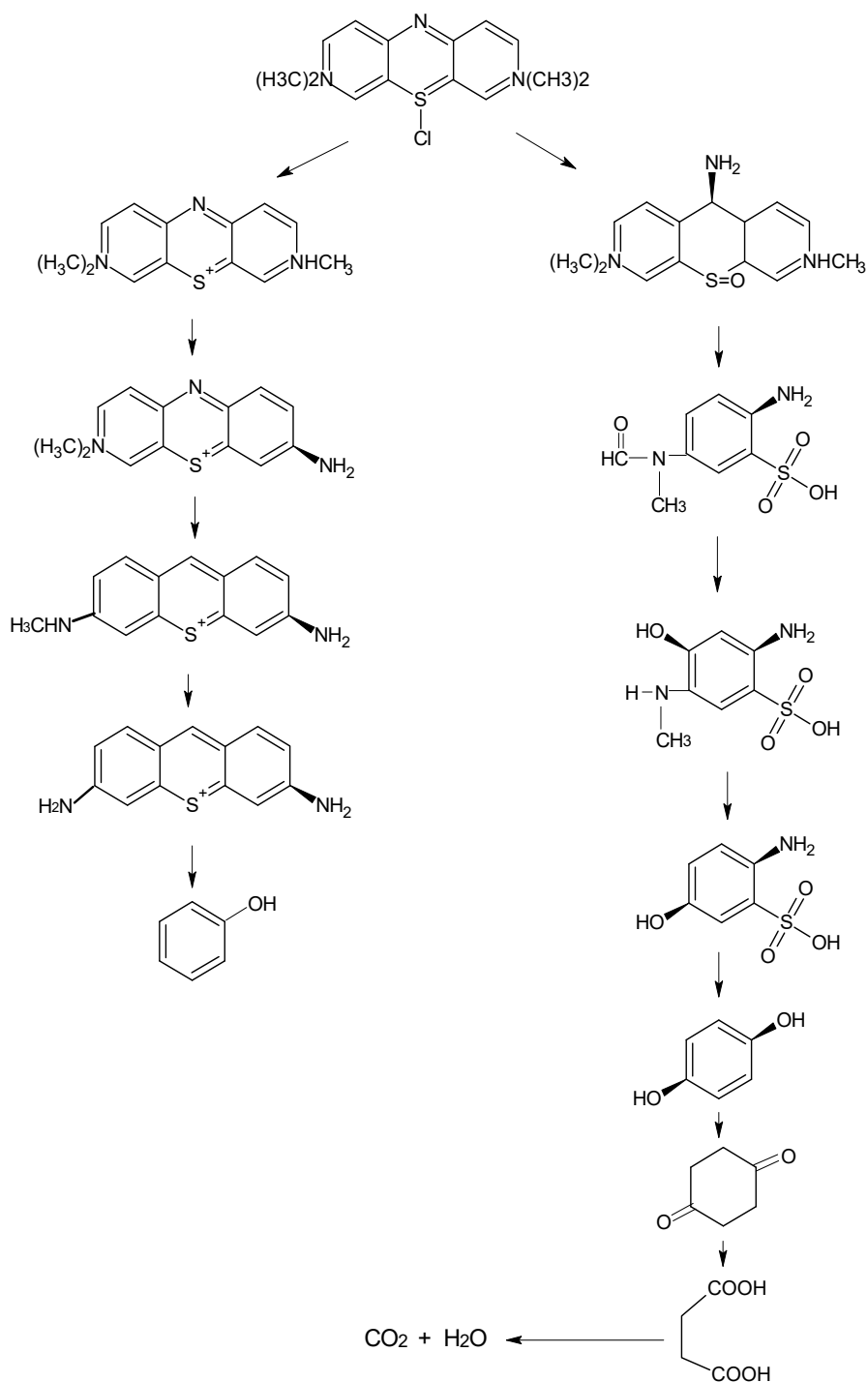


Figure 9. Possible degradation mechanism of MB based on MS spectra.

4.8.7. Auxochrome Group Degradation: Second Degradation Pathway

The investigators have identified various intermediate products during further mass spectroscopy analysis. Different intermediate compounds, including azure A ($m/z = 270$), azure B ($m/z = 256$), azure C ($m/z = 242$), and thionine ($m/z = 228$), that were produced during the PD due to demethylation cleavage, were identified [93]. The conjugation system between the two-dimethylamine-substituted aromatic rings through the S and N is responsible for the absorbance at 668 nm, while the small shoulder at 615 nm has been

reported to be due to the absorbance of dye dimer, whereas the substituted benzene rings have their absorbance peak in the UV region. The absorption peak at 668 nm diminished very fast. This indicated a rapid photocatalytic degradation of MB.

5. Conclusions

The synthesis of ZnONPs from vegetable waste suggests an economical and eco-friendly method. The development of ZnONPs and kaolin clay composite for the photocatalytic degradation of methylene blue provided an economical and eco-friendly approach. The developed clay nanocomposite was found to be rod-shaped and decorated with spherical ZnONPs, as revealed by FESEM and TEM. The average particle size of the nanocomposite was 54.24 ± 0.55 nm. The FTIR showed the presence of ZnO and Al-O, Si-O-Si groups in the nanocomposite. XRD has shown the diffraction peaks for both ZnONPs and kaolin, where the ZnONP peaks were from $33\text{--}44^\circ$ and for kaolin at 17 and 29° . The effect of various parameters on the photocatalytic degradation of MB dye shows efficient photocatalytic degradation. The photocatalyst efficiently degraded about 60–96% of MB dye in the aqueous solutions within a short period. The anchoring of ZnONPs in the kaolin matrix restricts the leaching of Zn into the environment without suppressing the photocatalytic potential of the ZnONPs.

Author Contributions: Conceptualization, S.M., D.A. and A.P.; Methodology, S.M., V.K.Y., S.A. and A.P.; Software, N.C. and D.K.S.; Validation, N.C., D.K.S. and M.H.F.; Formal analysis, N.C. and M.H.F.; Investigation, V.K.Y., S.M. and A.P.; Resources, D.A., S.A. and D.K.S.; Data curation, S.A. and M.H.F.; Writing—original draft, S.M., N.C. and V.K.Y.; Writing—review & editing, S.M., V.K.Y., D.A., N.C., S.A., D.K.S. and M.H.F.; Visualization, M.H.F. and V.K.Y.; Supervision, N.C. and A.P.; Project administration, V.K.Y., S.M., S.A. and A.P.; Funding acquisition, D.A., D.K.S. and S.A. All authors have read and agreed to the published version of the manuscript.

Funding: This research received no external funding.

Data Availability Statement: No new data were created or analyzed in this study. Data sharing is not applicable to this article.

Acknowledgments: This research was supported by the Researchers Supporting Project number (RSP2023R27), King Saud University, Riyadh, Saudi Arabia. The authors are thankful to the Department of Life Sciences for providing laboratory facilities and infrastructure.

Conflicts of Interest: The authors declare no conflict of interest.

References

- Islam, T.; Repon, M.R.; Islam, T.; Sarwar, Z.; Rahman, M.M. Impact of Textile Dyes on Health and Ecosystem: A Review of Structure, Causes, and Potential Solutions. *Environ. Sci. Pollut. Res.* **2023**, *30*, 9207–9242. [[CrossRef](#)] [[PubMed](#)]
- Al-Tohamy, R.; Ali, S.S.; Li, F.; Okasha, K.M.; Mahmoud, Y.A.-G.; Elsamahy, T.; Jiao, H.; Fu, Y.; Sun, J. A Critical Review on the Treatment of Dye-Containing Wastewater: Ecotoxicological and Health Concerns of Textile Dyes and Possible Remediation Approaches for Environmental Safety. *Ecotoxicol. Environ. Saf.* **2022**, *231*, 113160. [[CrossRef](#)] [[PubMed](#)]
- Pillai, S.B.; Thombre, N.V. Coagulation, Flocculation, and Precipitation in Water and Used Water Purification. In *Handbook of Water and Used Water Purification*; Lahnsteiner, J., Ed.; Springer International Publishing: Cham, Switzerland, 2020; pp. 1–25. ISBN 978-3-319-66382-1.
- Sreelekshmi, P.B.; Pillai, R.R.; Unnimaya, S.; Anju, A.L.; Meera, A.P. Biofabrication of Novel ZnO Nanoparticles for Efficient Photodegradation of Industrial Dyes. *Clean. Technol. Environ. Policy* **2023**. [[CrossRef](#)]
- Choudhary, N.; Chaudhari, J.; Mochi, V.; Patel, P.; Ali, D.; Alarifi, S.; Sahoo, D.K.; Patel, A.; Kumar Yadav, V. Phytonanofabrication of Copper Oxide by Albizia Saman and Their Potential as an Antimicrobial Agent and Remediation of Congo Red Dye from Wastewater. *Water* **2023**, *15*, 3787. [[CrossRef](#)]
- Gorbatshevich, O.B.; Kholodkov, D.N.; Kurkin, T.S.; Malakhova, Y.N.; Strel'tsov, D.R.; Buzin, A.I.; Kazakova, V.V.; Muzafarov, A.M.; Enikolopov, N.S. Synthesis and Properties of Watersoluble Silica Nanoparticles. *Russ. Chem. Bull.* **2017**, *66*, 409–417. [[CrossRef](#)]
- Mohan, A.; Jaison, A.; Lee, Y.-C. Emerging Trends in Mesoporous Silica Nanoparticle-Based Catalysts for CO₂ Utilization Reactions. *Inorg. Chem. Front.* **2023**, *10*, 3171–3194. [[CrossRef](#)]
- Tang, T.; Zhou, M.; Lv, J.; Cheng, H.; Wang, H.; Qin, D.; Hu, G.; Liu, X. Sensitive and Selective Electrochemical Determination of Uric Acid in Urine Based on Ultrasmall Iron Oxide Nanoparticles Decorated Urchin-like Nitrogen-Doped Carbon. *Colloids Surf. B Biointerfaces* **2022**, *216*, 112538. [[CrossRef](#)]

9. VafaeiAsl, M.; Keshavarz, I.; Shemirani, F.; Jamshidi, P. Green Synthesis of a Novel Magnetic $\text{Fe}_3\text{O}_4@\text{SiO}_2/\text{TiO}_2@\text{WO}_3$ Nanocomposite for Methylene Blue Removal under UV and Visible Light Irradiations. *Res. Chem. Intermed.* **2023**, *49*, 1909–1924. [CrossRef]
10. Liang, Y.; Li, J.; Xue, Y.; Tan, T.; Jiang, Z.; He, Y.; Shangguan, W.; Yang, J.; Pan, Y. Benzene Decomposition by Non-Thermal Plasma: A Detailed Mechanism Study by Synchrotron Radiation Photoionization Mass Spectrometry and Theoretical Calculations. *J. Hazard. Mater.* **2021**, *420*, 126584. [CrossRef]
11. Sun, S.; Liu, H.; Zhang, J.; Wang, W.; Xu, P.; Zhu, X.; Wang, Y.; Wan, S. Application of a Novel Coagulant in Reservoir Water Treatment in Qingdao. *Desalination Water Treat.* **2023**, *284*, 49–60. [CrossRef]
12. Ansari, M.A.H.; Khan, M.E.; Mohammad, A.; Baig, M.T.; Chaudary, A.; Tauqueer, M. 15—Application of Nanocomposites in Wastewater Treatment. In *Nanocomposites-Advanced Materials for Energy and Environmental Aspects*; Khan, M.E., Aslam, J., Verma, C., Eds.; Woodhead Publishing: Sawston, UK, 2023; pp. 297–319. ISBN 978-0-323-99704-1.
13. Zhang, J.; Zhong, A.; Huang, G.; Yang, M.; Li, D.; Teng, M.; Han, D. Enhanced Efficiency with CDCA Co-Adsorption for Dye-Sensitized Solar Cells Based on Metallosalophen Complexes. *Sol. Energy* **2020**, *209*, 316–324. [CrossRef]
14. Li, H.; Si, S.; Yang, K.; Mao, Z.; Sun, Y.; Cao, X.; Yu, H.; Zhang, J.; Ding, C.; Liang, H.; et al. Hexafluoroisopropanol Based Silk Fibroin Coatings on AZ31 Biometals with Enhanced Adhesion, Corrosion Resistance and Biocompatibility. *Prog. Org. Coat.* **2023**, *184*, 107881. [CrossRef]
15. Yan, F.; Jiang, J.; Li, K.; Liu, N.; Chen, X.; Gao, Y.; Tian, S. Green Synthesis of Nanosilica from Coal Fly Ash and Its Stabilizing Effect on CaO Sorbents for CO_2 Capture. *Environ. Sci. Technol.* **2017**, *51*, 7606–7615. [CrossRef]
16. Wang, Z.; Chen, C.; Liu, H.; Hrynnshpan, D.; Savitskaya, T.; Chen, J.; Chen, J. Enhanced Denitrification Performance of Alcaligenes SpTB by Pd Stimulating to Produce Membrane Adaptation Mechanism Coupled with Nanoscale Zero-Valent Iron. *Sci. Total Environ.* **2020**, *708*, 135063. [CrossRef] [PubMed]
17. Baig, N.; Kammakakam, I.; Falath, W. Nanomaterials: A Review of Synthesis Methods, Properties, Recent Progress, and Challenges. *Mater. Adv.* **2021**, *2*, 1821–1871. [CrossRef]
18. Tariq, A.; Bhawani, S.A.; Asaruddin, M.R.; Alotaibi, K.M. 2—Introduction to Nanocomposites. In *Polysaccharide-Based Nanocomposites for Gene Delivery and Tissue Engineering*; Bhawani, S.A., Karim, Z., Jawaid, M., Eds.; Woodhead Publishing: Sawston, UK, 2021; pp. 15–37. ISBN 978-0-12-821230-1.
19. Chen, D.; Wang, Q.; Li, Y.; Li, Y.; Zhou, H.; Fan, Y. A General Linear Free Energy Relationship for Predicting Partition Coefficients of Neutral Organic Compounds. *Chemosphere* **2020**, *247*, 125869. [CrossRef]
20. Zsirka, B.; Vágvölgyi, V.; Horváth, E.; Juzsakova, T.; Fónagy, O.; Szabó-bárdos, E.; Kristóf, J. Halloysite-Zinc Oxide Nanocomposites as Potential Photocatalysts. *Minerals* **2022**, *12*, 476. [CrossRef]
21. Chitra, M.; Mangamma, G.; Uthayarani, K.; Neelakandeswari, N.; Girija, E.K. Band Gap Engineering in ZnO Based Nanocomposites. *Phys. E Low. Dimens. Syst. Nanostruct.* **2020**, *119*, 113969. [CrossRef]
22. Shalan, A.E.; Makhlof, A.S.H.; Lanceros-Méndez, S. Nanocomposites Materials and Their Applications: Current and Future Trends. In *Advances in Nanocomposite Materials for Environmental and Energy Harvesting Applications*; Shalan, A.E., Hamdy Makhlof, A.S., Lanceros-Méndez, S., Eds.; Springer International Publishing: Cham, Switzerland, 2022; pp. 3–14. ISBN 978-3-030-94319-6.
23. Zahmatkesh, S.; Hajiaghaei-Kesheli, M.; Bokhari, A.; Sundaramurthy, S.; Panneerselvam, B.; Rezakhani, Y. Wastewater Treatment with Nanomaterials for the Future: A State-of-the-Art Review. *Environ. Res.* **2023**, *216*, 114652. [CrossRef]
24. Gnanamoorthy, G.; Yadav, V.K.; Ali, D.; Ramar, K.; Ali, H.; Narayanan, V. New Designing $(\text{NH}_4)_2\text{SiP}_4\text{O}_{13}$ Nanowires and Effective Photocatalytic Degradation of Malachite Green. *Chem. Phys. Lett.* **2022**, *803*, 139817. [CrossRef]
25. Kong, L.; Liu, Y.; Dong, L.; Zhang, L.; Qiao, L.; Wang, W.; You, H. Enhanced Red Luminescence in $\text{CaAl}_2\text{O}_1:\text{Mn}^{4+}$ via Doping Ga^{3+} for Plant Growth Lighting. *Dalton Trans.* **2020**, *49*, 1947–1954. [CrossRef]
26. Liu, W.; Zhao, C.; Zhou, Y.; Xu, X. Modeling of Vapor-Liquid Equilibrium for Electrolyte Solutions Based on COSMO-RS Interaction. *J. Chem.* **2022**, *2022*, 9070055. [CrossRef]
27. Al-Attar, H.M.; Hussein, H.T.; Zamel, R.S.; Addie, A.J.; Mohammed, M.K.A. Methylene Blue Degradation Using $\text{ZnO}:\text{CuO}:\text{Al}_2\text{O}_3$ Nanocomposite Synthesized by Liquid Laser Ablation. *Opt. Quantum. Electron.* **2023**, *55*, 309. [CrossRef]
28. Shan, L.; Tan, C.Y.; Shen, X.; Ramesh, S.; Zarei, M.S.; Kolahchi, R.; Hajmohammad, M.H. The Effects of Nano-Additives on the Mechanical, Impact, Vibration, and Buckling/Post-Buckling Properties of Composites: A Review. *J. Mater. Res. Technol.* **2023**, *24*, 7570–7598. [CrossRef]
29. Ghazanlou, S.I.; Ghazanlou, S.I.; Ashraf, W. Improvement in the Physical and Mechanical Properties of the Cement-Based Composite with the Addition of Nanostructured BN- Fe_3O_4 Reinforcement. *Sci. Rep.* **2021**, *11*, 19358. [CrossRef]
30. Sharma, D.; Kumar, M.; Jain, V.P.; Chaudhary, S.; Jaiswar, G. Bio-Based Polyamide Nanocomposites of Nanoclay, Carbon Nanotubes and Graphene: A Review. *Iran. Polym. J.* **2023**, *32*, 773–790. [CrossRef]
31. Zhang, G.; Zhao, Z.; Yin, X.-A.; Zhu, Y. Impacts of Biochars on Bacterial Community Shifts and Biodegradation of Antibiotics in an Agricultural Soil during Short-Term Incubation. *Sci. Total Environ.* **2021**, *771*, 144751. [CrossRef] [PubMed]
32. Temga, J.P.; Mache, J.R.; Madi, A.B.; Nguetnkam, J.P.; Bitom, D.L. Ceramics Applications of Clay in Lake Chad Basin, Central Africa. *Appl. Clay Sci.* **2019**, *171*, 118–132. [CrossRef]
33. Giese, R.F. Kaolin Group Minerals. In *Encyclopedia of Sediments and Sedimentary Rocks*; Middleton, G.V., Church, M.J., Coniglio, M., Hardie, L.A., Longstaffe, F.J., Eds.; Springer: Dordrecht, The Netherlands, 2003; pp. 398–400. ISBN 978-1-4020-3609-5.
34. Murray, H.; Kogel, J.E. Engineered Clay Products for the Paper Industry. *Appl. Clay Sci.* **2005**, *29*, 199–206. [CrossRef]

35. Hadia, N.J.; Ng, Y.H.; Stubbs, L.P.; Torsæter, O. High Salinity and High Temperature Stable Colloidal Silica Nanoparticles with Wettability Alteration Ability for EOR Applications. *Nanomaterials* **2021**, *11*, 707. [[CrossRef](#)]
36. Mochizuki, C.; Nakamura, J.; Nakamura, M. Development of Non-Porous Silica Nanoparticles towards Cancer Photo-Theranostics. *Biomedicines* **2021**, *9*, 73. [[CrossRef](#)]
37. Kloprogge, J. The Kaolin Group: Octahedral and Tetrahedral Sheets. In *Spectroscopic Methods in the Study of Kaolin Minerals and Their Modifications*; Kloprogge, J., Ed.; Springer International Publishing: Cham, Switzerland, 2019; pp. 97–159. ISBN 978-3-030-02373-7.
38. Caponi, N.; Collazzo, G.C.; Jahn, S.L.; Dotto, G.L.; Mazutti, M.A.; Foletto, E.L. Use of Brazilian Kaolin as a Potential Low-Cost Adsorbent for the Removal of Malachite Green from Colored Effluents. *Mater. Res.* **2017**, *20*, 14–22.
39. Ibrahim, H.; Mahmoud, T.; Hegazy, E. Application of Zeolite Prepared from Egyptian Kaolin for the Removal of Heavy Metals: II. Isotherm Models. *J. Hazard. Mater.* **2010**, *182*, 842–847. [[CrossRef](#)]
40. Valášková, M.; Blahúšková, V.; Vlček, J. Effects of Kaolin Additives in Fly Ash on Sintering and Properties of Mullite Ceramics. *Minerals* **2021**, *11*, 887. [[CrossRef](#)]
41. Gougazeh, M.; Buhl, J.-C. Synthesis and Characterization of Zeolite A by Hydrothermal Transformation of Natural Jordanian Kaolin. *J. Assoc. Arab. Univ. Basic Appl. Sci.* **2014**, *15*, 35–42. [[CrossRef](#)]
42. Babayevska, N.; Przysiecka, Ł.; Iatsunskyi, I.; Nowaczyk, G.; Jarek, M.; Janiszewska, E.; Jurga, S. ZnO Size and Shape Effect on Antibacterial Activity and Cytotoxicity Profile. *Sci. Rep.* **2022**, *12*, 8148. [[CrossRef](#)]
43. Peres, L.G.S.; Malafatti, J.O.D.; Bernardi, B.; Mattoso, L.H.C.; Paris, E.C. Biodegradable Starch Sachets Reinforced with Montmorillonite for Packing ZnO Nanoparticles: Solubility and Zn²⁺ Ions Release. *J. Polym. Environ.* **2023**, *31*, 2388–2398. [[CrossRef](#)]
44. Shu, Z.; Zhang, Y.; Yang, Q.; Yang, H. Halloysite Nanotubes Supported Ag and ZnO Nanoparticles with Synergistically Enhanced Antibacterial Activity. *Nanoscale Res. Lett.* **2017**, *12*, 135. [[CrossRef](#)]
45. Peng, H.; Liu, X.; Tang, W.; Ma, R. Facile Synthesis and Characterization of ZnO Nanoparticles Grown on Halloysite Nanotubes for Enhanced Photocatalytic Properties. *Sci. Rep.* **2017**, *7*, 2250. [[CrossRef](#)]
46. Choudhary, N.; Yadav, V.K.; Ali, H.; Ali, D.; Almutairi, B.O.; Cavalu, S.; Patel, A. Remediation of Methylene Blue Dye from Wastewater by Using Zinc Oxide Nanoparticles Loaded on Nanoclays. *Water* **2023**, *15*, 1427. [[CrossRef](#)]
47. Meigoli Boushehrian, M.; Esmaeili, H.; Foroutan, R. Ultrasonic Assisted Synthesis of Kaolin/CuFe₂O₄ Nanocomposite for Removing Cationic Dyes from Aqueous Media. *J. Environ. Chem. Eng.* **2020**, *8*, 103869. [[CrossRef](#)]
48. Choudhary, N.; Yadav, V.K.; Yadav, K.K.; Almohana, A.I.; Almojil, S.F.; Gnanamoorthy, G.; Kim, D.-H.; Islam, S.; Kumar, P.; Jeon, B.-H. Application of Green Synthesized MMT/Ag Nanocomposite for Removal of Methylene Blue from Aqueous Solution. *Water* **2021**, *13*, 3206. [[CrossRef](#)]
49. Gnanamoorthy, G.; Karthikeyan, V.; Ali, D.; Kumar, G.; Yadav, V.K.; Narayanan, V. Global Popularization of CuNiO₂ and Their RGO Nanocomposite Loveable to the Photocatalytic Properties of Methylene Blue. *Environ. Res.* **2022**, *204*, 112338. [[CrossRef](#)]
50. Bayomie, O.S.; Kandeel, H.; Shoeib, T.; Yang, H.; Youssef, N.; El-Sayed, M.M.H. Novel Approach for Effective Removal of Methylene Blue Dye from Water Using Fava Bean Peel Waste. *Sci. Rep.* **2020**, *10*, 7824. [[CrossRef](#)]
51. Massaro, M.; Casiello, M.; D'Accolti, L.; Lazzara, G.; Nacci, A.; Nicotra, G.; Noto, R.; Pettignano, A.; Spinella, C.; Riela, S. One-Pot Synthesis of ZnO Nanoparticles Supported on Halloysite Nanotubes for Catalytic Applications. *Appl. Clay Sci.* **2020**, *189*, 105527. [[CrossRef](#)]
52. Mustapha, S.; Tijani, J.O.; Ndamitso, M.M.; Abdulkareem, S.A.; Shuaib, D.T.; Mohammed, A.K.; Sumaila, A. The Role of Kaolin and Kaolin/ZnO Nanoadsorbents in Adsorption Studies for Tannery Wastewater Treatment. *Sci. Rep.* **2020**, *10*, 13068. [[CrossRef](#)] [[PubMed](#)]
53. Mamulová Kutláková, K.; Tokarský, J.; Peikertová, P. Functional and Eco-Friendly Nanocomposite Kaolinite/ZnO with High Photocatalytic Activity. *Appl. Catal. B* **2015**, *162*, 392–400. [[CrossRef](#)]
54. Modi, S.; Yadav, V.K.; Amari, A.; Osman, H.; Igwegbe, C.A.; Fulekar, M.H. Nanobioremediation: A Bacterial Consortium-Zinc Oxide Nanoparticle-Based Approach for the Removal of Methylene Blue Dye from Wastewater. *Environ. Sci. Pollut. Res.* **2023**, *30*, 72641–72651. [[CrossRef](#)]
55. Modi, S.; Yadav, V.K.; Amari, A.; Alyami, A.Y.; Gacem, A.; Harharah, H.N.; Fulekar, M.H. Photocatalytic Degradation of Methylene Blue Dye from Wastewater by Using Doped Zinc Oxide Nanoparticles. *Water* **2023**, *15*, 2275. [[CrossRef](#)]
56. Modi, S.; Fulekar, M.H. Green Synthesis of Zinc Oxide Nanoparticles Using Garlic Skin Extract and Its Characterization. *J. Nanostruct.* **2020**, *10*, 20–27. [[CrossRef](#)]
57. Melguizo-Rodríguez, L.; García-Recio, E.; Ruiz, C.; De Luna-Bertos, E.; Illescas-Montes, R.; Costela-Ruiz, V.J. Biological Properties and Therapeutic Applications of Garlic and Its Components. *Food Funct.* **2022**, *13*, 2415–2426. [[CrossRef](#)]
58. dos Santos, P.C.M.; da Silva, L.M.R.; Magalhaes, F.E.A.; Cunha, F.E.T.; Ferreira, M.J.G.; de Figueiredo, E.A.T. Garlic (*Allium sativum* L.) Peel Extracts: From Industrial by-Product to Food Additive. *Appl. Food Res.* **2022**, *2*, 100186. [[CrossRef](#)]
59. Hernández-Montesinos, I.Y.; Carreón-Delgado, D.F.; Ocaranza-Sánchez, E.; Ochoa-Velasco, C.E.; Suárez-Jacobo, Á.; Ramírez-López, C. Garlic (*Allium sativum*) Peel Extracts and Their Potential as Antioxidant and Antimicrobial Agents for Food Applications: Influence of Pretreatment and Extraction Solvent. *Int. J. Food Sci. Technol.* **2023**. [[CrossRef](#)]
60. Rahaman, M.Z.; Akther Hossain, A.K.M. Effect of Metal Doping on the Visible Light Absorption, Electronic Structure and Mechanical Properties of Non-Toxic Metal Halide CsGeCl₃. *RSC Adv.* **2018**, *8*, 33010–33018. [[CrossRef](#)]

61. Amendola, V.; Pilot, R.; Frasconi, M.; Maragò, O.M.; Iati, M.A. Surface Plasmon Resonance in Gold Nanoparticles: A Review. *J. Phys. Condens. Matter* **2017**, *29*, 203002. [[CrossRef](#)]
62. Khan, S.H.; Pathak, B.; Fulekar, M.H. Synthesis, Characterization and Photocatalytic Degradation of Chlorpyrifos by Novel Fe: ZnO Nanocomposite Material. *Nanotechnol. Environ. Eng.* **2018**, *3*, 13. [[CrossRef](#)]
63. Aluvihara, S.; Kalpage, C.S.; Lemle, K.L. Elementary Chemical Analysis of Different Clay Types. *J. Phys. Conf. Ser.* **2021**, *1781*, 012007. [[CrossRef](#)]
64. Bordeepong, S.; Bhongsuwan, D.; Punggrassami, T.; Bhongsuwan, T. Mineralogy, Chemical Composition and Ceramic Properties of Clay Deposits in Southern Thailand. *Agric. Nat. Resour.* **2012**, *46*, 485–500.
65. Biswas, B.; Labille, J.; Prelot, B. Clays and Modified Clays in Remediating Environmental Pollutants. *Environ. Sci. Pollut. Res.* **2020**, *27*, 38381–38383. [[CrossRef](#)] [[PubMed](#)]
66. Amar, A.; Loulidi, I.; Kali, A.; Boukhli, F.; Hadey, C.; Jabri, M. Physicochemical Characterization of Regional Clay: Application to Phenol Adsorption. *Appl. Environ. Soil. Sci.* **2021**, *2021*, 8826063. [[CrossRef](#)]
67. Mustapha, S.; Tijani, J.O.; Ndamitso, M.M.; Abdulkareem, A.S.; Shuaib, D.T.; Mohammed, A.K. A Critical Review on Geosmin and 2-Methylisoborneol in Water: Sources, Effects, Detection, and Removal Techniques. *Environ. Monit. Assess.* **2021**, *193*, 204. [[CrossRef](#)]
68. Modi, S.; Fulekar, M.H. Synthesis and Characterization of Zinc Oxide Nanoparticles and Zinc Oxide/Cellulose Nanocrystals Nanocomposite for Photocatalytic Degradation of Methylene Blue Dye under Solar Light Irradiation. *Nanotechnol. Environ. Eng.* **2020**, *5*, 18. [[CrossRef](#)]
69. Saied, E.; Salem, S.S.; Al-Askar, A.A.; Elkady, F.M.; Arishi, A.A.; Hashem, A.H. Mycosynthesis of Hematite (α -Fe₂O₃) Nanoparticles Using Aspergillus Niger and Their Antimicrobial and Photocatalytic Activities. *Bioengineering* **2022**, *9*, 397. [[CrossRef](#)] [[PubMed](#)]
70. Ahamed Khan, M.; Lone, S.A.; Shahid, M.; Zeyad, M.T.; Syed, A.; Ehtram, A.; Elgorban, A.M.; Verma, M.; Danish, M. Phytogenically Synthesized Zinc Oxide Nanoparticles (ZnO-NPs) Potentially Inhibit the Bacterial Pathogens: In Vitro Studies. *Toxics* **2023**, *11*, 452. [[CrossRef](#)] [[PubMed](#)]
71. Yang, D.; Wang, Y.; Chen, C.; Su, Y.; Li, L.; Miao, L.; Gu, H.; Zhao, W.; Ding, L.; Hu, D. Oriented Plate-like KNbO₃ Polycrystals: Topochemical Mesocrystal Conversion and Piezoelectric and Photocatalytic Responses. *Inorg. Chem.* **2023**, *62*, 10408–10419. [[CrossRef](#)]
72. Zheng, Y.; Liu, Y.; Guo, X.; Chen, Z.; Zhang, W.; Wang, Y.; Tang, X.; Zhang, Y.; Zhao, Y. Sulfur-Doped g-C₃N₄/RGO Porous Nanosheets for Highly Efficient Photocatalytic Degradation of Refractory Contaminants. *J. Mater. Sci. Technol.* **2020**, *41*, 117–126. [[CrossRef](#)]
73. Yu, H.; Zhu, J.; Qiao, R.; Zhao, M.; Kong, L. Facile Preparation and Controllable Absorption of a Composite Based on PMo12/Ag Nanoparticles: Photodegradation Activity and Mechanism. *ChemistrySelect* **2022**, *7*, e202103668. [[CrossRef](#)]
74. Meky, A.I.; Hassaan, M.A.; Fetouh, H.A.; Ismail, A.M.; El Nemr, A. Cube-Shaped Cobalt-Doped Zinc Oxide Nanoparticles with Increased Visible-Light-Driven Photocatalytic Activity Achieved by Green Co-Precipitation Synthesis. *Sci. Rep.* **2023**, *13*, 19329. [[CrossRef](#)] [[PubMed](#)]
75. Tsade Kara, H.; Anshebo, S.T.; Sabir, F.K.; Adam Workineh, G. Removal of Methylene Blue Dye from Wastewater Using Periodiated Modified Nanocellulose. *Int. J. Chem. Eng.* **2021**, *2021*, 9965452. [[CrossRef](#)]
76. Behnajady, M.A.; Modirshahla, N.; Hamzavi, R. Kinetic Study on Photocatalytic Degradation of C.I. Acid Yellow 23 by ZnO Photocatalyst. *J. Hazard. Mater.* **2006**, *133*, 226–232. [[CrossRef](#)]
77. Badeenezhad, A.; Azhdarpoor, A.; Bahrami, S.; Yousefinejad, S. Removal of Methylene Blue Dye from Aqueous Solutions by Natural Clinoptilolite and Clinoptilolite Modified by Iron Oxide Nanoparticles. *Mol. Simul.* **2019**, *45*, 564–571. [[CrossRef](#)]
78. Albarakaty, F.M.; Alzaban, M.I.; Alharbi, N.K.; Bagrwan, F.S.; Abd El-Aziz, A.R.M.; Mahmoud, M.A. Zinc Oxide Nanoparticles, Biosynthesis, Characterization and Their Potent Photocatalytic Degradation, and Antioxidant Activities. *J. King Saud Univ. Sci.* **2023**, *35*, 102434. [[CrossRef](#)]
79. Yadav, V.K.; Choudhary, N.; Ali, D.; Kumar, G.; Gnanamoorthy, G.; Khan, A.U.; Kumar, P.; Hari Kumar, S.; Tizazu, B.Z. Determination of Adsorption of Methylene Blue Dye by Incense Stick Ash Waste and Its Toxicity on RTG-2 Cells. *Adsorpt. Sci. Technol.* **2022**, *2022*, 8565151. [[CrossRef](#)]
80. Zhang, Y.; Zhao, M.; Huang, J.; Zhao, N.; Yu, H. Controllable Synthesis, Photocatalytic Property, and Mechanism of a Novel POM-Based Direct Z-Scheme Nano-Heterojunction α -Fe₂O₃/P2Mo18. *Molecules* **2023**, *28*, 6671. [[CrossRef](#)] [[PubMed](#)]
81. Ai, L.; Jiang, J. Removal of Methylene Blue from Aqueous Solution with Self-Assembled Cylindrical Graphene–Carbon Nanotube Hybrid. *Chem. Eng. J.* **2012**, *192*, 156–163. [[CrossRef](#)]
82. Mir, I.A.; Singh, I.; Birajdar, B.; Rawat, K. A Facile Platform for Photocatalytic Reduction of Methylene Blue Dye by CdSe-TiO₂ Nanoparticles. *Water Conserv. Sci. Eng.* **2017**, *2*, 43–50. [[CrossRef](#)]
83. Tran, H.V.; Bui, L.T.; Dinh, T.T.; Le, D.H.; Huynh, C.D.; Trinh, A.X. Graphene Oxide/Fe₃O₄/Chitosan Nanocomposite: A Recoverable and Recyclable Adsorbent for Organic Dyes Removal. Application to Methylene Blue. *Mater. Res. Express* **2017**, *4*, 035701. [[CrossRef](#)]
84. Bangari, R.S.; Yadav, A.; Bharadwaj, J.; Sinha, N. Boron Nitride Nanosheets Incorporated Polyvinylidene Fluoride Mixed Matrix Membranes for Removal of Methylene Blue from Aqueous Stream. *J. Environ. Chem. Eng.* **2022**, *10*, 107052. [[CrossRef](#)]

85. Tarekegn, M.M.; Balakrishnan, R.M.; Hiruy, A.M.; Dekebo, A.H. Removal of Methylene Blue Dye Using Nano Zerovalent Iron, Nanoclay and Iron Impregnated Nanoclay—A Comparative Study. *RSC Adv.* **2021**, *11*, 30109–30131. [[CrossRef](#)]
86. Fouada, A.; Salem, S.S.; Wassel, A.R.; Hamza, M.F.; Shaheen, T.I. Optimization of Green Biosynthesized Visible Light Active CuO/ZnO Nano-Photocatalysts for the Degradation of Organic Methylene Blue Dye. *Heliyon* **2020**, *6*, e04896. [[CrossRef](#)]
87. Fan, J.; Zhang, B.; Zhu, B.; Shen, W.; Chen, Y.; Zeng, F. New Insight into the Mechanism for the Removal of Methylene Blue by Hydrotalcite-Supported Nanoscale Zero-Valent Iron. *Water* **2023**, *15*, 183. [[CrossRef](#)]
88. Nazir, M.A.; Khan, N.A.; Cheng, C.; Shah, S.S.A.; Najam, T.; Arshad, M.; Sharif, A.; Akhtar, S.; Rehman, A. Ur Surface Induced Growth of ZIF-67 at Co-Layered Double Hydroxide: Removal of Methylene Blue and Methyl Orange from Water. *Appl. Clay Sci.* **2020**, *190*, 105564. [[CrossRef](#)]
89. Khan, S.B.; Khan, M.I.; Nisar, J. Microwave-Assisted Green Synthesis of Pure and Mn-Doped ZnO Nanocomposites: In Vitro Antibacterial Assay and Photodegradation of Methylene Blue. *Front. Mater.* **2022**, *8*, 710155. [[CrossRef](#)]
90. Jamshaid, M.; Nazir, M.A.; Najam, T.; Shah, S.S.A.; Khan, H.M.; Rehman, A. ur Facile Synthesis of Yb³⁺-Zn²⁺ Substituted M Type Hexaferrites: Structural, Electric and Photocatalytic Properties under Visible Light for Methylene Blue Removal. *Chem. Phys. Lett.* **2022**, *805*, 139939. [[CrossRef](#)]
91. Jana, T.K.; Chatterjee, K. Hybrid Nanostructures Exhibiting Both Photocatalytic and Antibacterial Activity—A Review. *Environ. Sci. Pollut. Res.* **2023**, *30*, 95215–95249. [[CrossRef](#)] [[PubMed](#)]
92. Cinelli, G.; Cuomo, F.; Ambrosone, L.; Colella, M.; Ceglie, A.; Venditti, F.; Lopez, F. Photocatalytic Degradation of a Model Textile Dye Using Carbon-Doped Titanium Dioxide and Visible Light. *J. Water Process Eng.* **2017**, *20*, 71–77. [[CrossRef](#)]
93. Ablikim, M.; Achasov, M.N.; Ahmed, S.; Albrecht, M.; Alekseev, M.; Amoroso, A.; An, F.F.; An, Q.; Bai, J.Z.; Bai, Y.; et al. Measurement of the Absolute Branching Fraction of the Inclusive Decay $\Lambda c^+ \rightarrow \Lambda + X$. *Phys. Rev. Lett.* **2018**, *121*, 062003. [[CrossRef](#)]

Disclaimer/Publisher’s Note: The statements, opinions and data contained in all publications are solely those of the individual author(s) and contributor(s) and not of MDPI and/or the editor(s). MDPI and/or the editor(s) disclaim responsibility for any injury to people or property resulting from any ideas, methods, instructions or products referred to in the content.